energies

MDPI

Article

Impedance Matching-Based Power Flow Analysis for UPQC in Three-Phase Four-Wire Systems

Xiaojun Zhao *, Xiuhui Chai, Xiaoqiang Guo, Ahmad Waseem, Xiaohuan Wang and Chunjiang Zhang

School of Electrical Engineering, Yanshan University, Qinhuangdao 066004, China; caixiuhuihb@126.com (X.C.); gxq@ysu.edu.cn (X.G.); wasim1081@gmail.com (A.W.); wxh@ysu.edu.cn (X.W.); zhangcj@ysu.edu.cn (C.Z.)
* Correspondence: zhaoxiaojun@ysu.edu.cn

Abstract: Different from the extant power flow analysis methods, this paper discusses the power flows for the unified power quality conditioner (UPQC) in three-phase four-wire systems from the point of view of impedance matching. To this end, combined with the designed control strategies, the establishing method of the UPQC impedance model is presented, and on this basis, the UPQC system can be equivalent to an adjustable impedance model. After that, a concept of impedance matching is introduced into this impedance model to study the operation principle for the UPQC system, i.e., how the system changes its operation states and power flow under the grid voltage variations through discussing the matching relationships among node impedances. In this way, the nodes of the series and parallel converter are matched into two sets of impedances in opposite directions, which mean that one converter operates in rectifier state to draw the energy and the other one operates in inverter state to transmit the energy. Consequently, no matter what grid voltages change, the system node impedances are dynamically matched to ensure that output equivalent impedances are always equal to load impedances, so as to realize impedance and power balances of the UPQC system. Finally, the correctness of the impedance matching-based power flow analysis is validated by the experimental results.

Keywords: UPQC; impedance model; impedance matching; power flow; operation states

Citation: Zhao, X.; Chai, X.; Guo, X.; Waseem, A.; Wang, X.; Zhang, C. Impedance Matching-Based Power Flow Analysis for UPQC in Three-Phase Four-Wire Systems. *Energies* **2021**, *14*, 2702. https://doi.org/10.3390/en14092702

Academic Editor: Lluís Monjo

Received: 19 April 2021
Accepted: 5 May 2021
Published: 8 May 2021

1. Introduction

Nowadays, the three-phase four-wire (3P4W) power supply system has been widely used in low-voltage distribution networks (LVDNs) because of its more flexible voltage supply mode [1], that is, it can provide consumers with 220 V phase voltage and 380 V line voltage. However, due to issues such as the start-up of impact load equipment, the randomness of the grid-connected output power of renewable energy, and the short-circuit failure of power systems [2], the 3P4W distribution networks mainly face the problem of grid voltage fluctuations (i.e., sag/swell), which may cause data loss or even damage to critical loads [3], such as financial industry computers, network servers, etc.

In order to protect the LVDNs and critical loads, the unified power quality conditioner (UPQC) [4] is increasingly used to improve the power quality problems in LVDNs. Usually, the UPQC, consisting of a series converter (SC) and a parallel converter (PC), can solve both voltage and current power quality problems, such as voltage variations, unbalance and harmonics as well as current power factors, unbalance and harmonics.

When the grid voltages change, to balance the active powers between grid side and load side, the UPQC system will switch the operation states of the SC and PC, that is, the SC/PC will be changed from a rectifier to an inverter or vice versa. Correspondingly, the amplitudes and directions of the power flows will be changed with the SC/PC's operation state changes. According to the phase angle difference between system output voltage (i.e., load voltage) and grid voltage, the common analysis methods of the UPQC's operation principle are as follows: (1) UPQC-P: the difference is 0 or π, the SC only transmits active

powers in the forward or reverse direction [5,6]; (2) UPQC-Q: the difference is $\pi/2$, the SC only transmits reactive powers for loads [7,8]; (3) UPQC-VAmin: the difference range is 0–$\pi/2$, the SC transmits active and reactive powers at the same time. This method attempts to minimize the volt-ampere (VA) loading, thereby reducing the design cost of UPQC [9,10]; (4) UPQC-S: it has the same range of the angle difference as UPQC-VAmin, but the difference is that the SC operates at maximum capacity to enhance the UPQC's utilization [11,12].

Hitherto the UPQC's operation principle has been rarely analyzed from the perspectives of the impedance model and impedance matching in previously published UPQC studies. For this objective, the concept of impedance matching was involved in the UPQC system in this paper, and the internal power flows of the system were analyzed by discussing the matching relationships among node impedances. However, the major challenges faced by this paper are how to establish the UPQC system's impedance model and how to use this model to analyze the power flows.

The impedance model has been widely used in system stability analysis, power sharing, power transmission and so on. In [13], the grid-connected converter is equivalent to a current source in parallel with an output impedance, and then the stability of the grid-connected converter is discussed by analyzing the impedance relationship between the converter and the gird. In [14], considering the influence of distributed capacitances of the transmission line and the transformer, the impedance model was utilized to analyze the harmonic resonance problem of the series-parallel hybrid active power filter (HAPF). In [15], the impedance model of thyristor-controlled LC-coupling HAPF is established, and the firing angles of thyristors are calculated to balance and compensate active and reactive power. In [16], the influence of line impedance between multiple distributed generations (DGs) and the point of common coupling (PCC) on the power distribution is analyzed, and then a power-sharing control method based on the virtual complex impedance is investigated to achieve accurate power-sharing between DGs. In [17], the equivalent impedance circuit of a unified power flow controller (UPFC) is established, and the active and reactive powers between the two power grids are adjusted by matching the impedance of UPFC and the transmission line.

Inspired by Refs. [13–17], Ref. [18] introduces the impedance matching into the UPQC and analyzes the impedance regulation process with three-phase unbalanced loads. However, the establishing method of the impedance model that plays a key role in impedance matching analysis is not given in Ref. [18]. In addition, in view of the fact that the establishing method of the UPQC impedance model is presented for the first time in this paper, the three-phase balanced loads are used as a research condition to verify the correctness of this method, and the corresponding relationships between node impedances and power flows are more clearly demonstrated.

In this paper, considering the operating characteristics of the two converters in terms of voltage- and current-source control methods, the SC can be equivalent to a controllable sinusoidal current source in parallel with its impedance, and the PC can be equivalent to a controllable sinusoidal voltage source in series with its impedance. In this way, the UPQC system is equivalent to an adjustable impedance model with five nodes (i.e., input node, SC node, node behind transformer, PC node and output node), in which the amplitude and direction of the node impedance, respectively, reflect the amplitude and direction of the power flow at the corresponding node. Once the grid voltages change, the original matching state of these node impedances will be broken, and then they will be re-adjusted to change the amplitudes and/or directions of power flows inside the system, so as to balance the active powers between input side (i.e., the grid side) and output side (i.e., the load side). As a result, no matter what grid voltages change, the system node impedances are dynamically matched to ensure that the output equivalent impedances are always equal to load impedances. Not only that, these node impedances will indicate two main characteristics as follows: (1) all node impedances are associated with load impedances; (2) except for the equivalent output impedance, four other impedances are associated

with the variation degree of grid voltages. Therefore, it is helpful to intuitively observe the factors that affect the system's power flows by means of this impedance model. In other words, the UPQC impedance model established in this paper can directly reflect the changing degrees of the grid voltage and load impedance to the system power flows.

The rest of this paper is organized as follows: Section 2, the control strategies of the UPQC system are designed and the equivalent impedance model is established. Section 3, the operation principle of the system is exhaustively analyzed from the power flow and impedance matching perspective. Section 4, theoretical calculation results of the voltages, currents, active powers and node impedances are obtained according to the impedance matching method. Finally, the correctness of the impedance matching-based power flow analysis is validated by the experimental results in Section 5.

2. Control Strategy and Impedance Model

To discuss the impedance matching, the UPQC's impedance model is an essential prerequisite. For this purpose, the control strategy of the UPQC system is designed in this section, and on this basis, the establishment process of the system's equivalent impedance model with five nodes is given in detail. Figure 1 shows the 3P4W UPQC's circuit topology, and its electrical quantities are shown in Table 1. In which, the antiparallel thyristors S_{abc} are used to disconnect the UPQC from the grid in the case of a grid short-circuit, power outage or other failures.

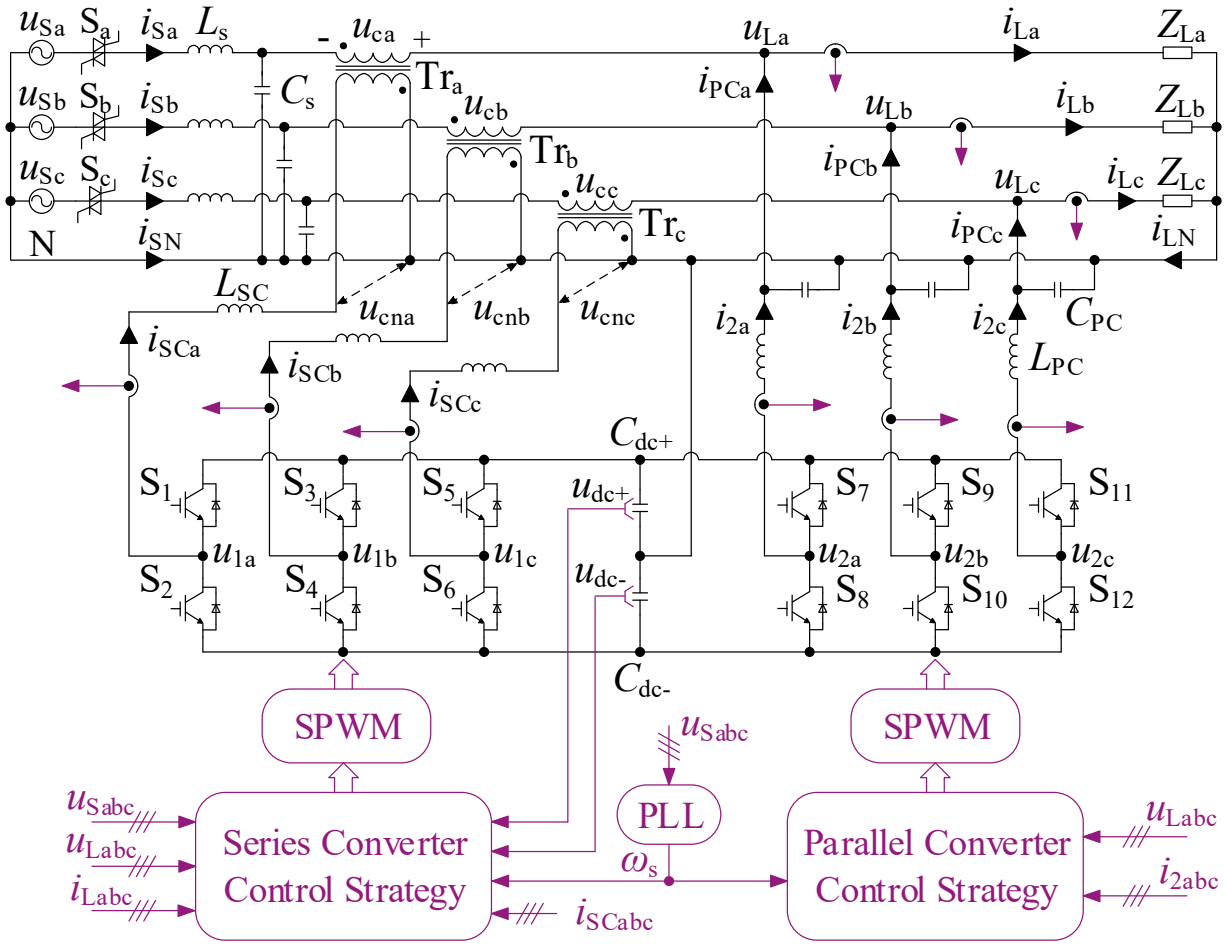

Figure 1. Three-phase four-wire UPQC configuration.

Table 1. Electrical quantities and specifications.

Quantity	Specification	Quantity	Specification
Thyristors	S_{abc}	PC IGBT switches	S_7~S_{12}
Grid voltages	u_{Sabc}	PC leg voltages	u_{2abc}
Grid currents	i_{Sabc}	Currents of L_{PC}	i_{2abc}
SC IGBT switches	S_1~S_6	PC output currents	i_{PCabc}
SC leg voltages	u_{1abc}	Load voltages	u_{Labc}
SC output currents	i_{SCabc}	Load currents	i_{Labc}
Series transformers	Tr_{abc}	Neutral line	N
Primary voltages of Tr_{abc}	u_{Cabc}	Load impedances	Z_{Labc}
Secondary voltages of Tr_{abc}	u_{Cnabc}	Grid side filter inductances	L_s = 6 μH
Grid side filter capacitors	C_s = 40 μF	SC side filter inductances	L_{SC} = 7 mH
Voltage ratio of Tr_{abc}	n = 1:5	PC side filter inductances	L_{PC} = 0.3 mH
Switching frequency of SC and PC	f_{sw} = 15 kHz	PC side filter capacitors	C_{PC} = 40 μF
Positive and negative dc-link capacitors	$C_{dc\pm}$ = 8800 μF	Positive and negative dc-link voltages	$u_{dc\pm}$ = ±400 V
Grid frequency	ω_s= 2π50 rad/s		

2.1. Series Converter Control Strategy and Impedance Model

The SC operates as a controllable sinusoidal current source, and Figure 2 shows its control block diagram in the *dq0*-frame, where ω_s can be obtained by a phase-locked loop (PLL) [19]. The dc-link voltage control and the active power balance (APB) principle [20] are employed to the generate grid current reference i^*_{Sd}, where the dc-link voltage control quantity i^*_{Sd1} is used to stabilize the dc-link voltage, also to compensate for system loss, while the APB generation quantity i^*_{Sd2} is responsible for generating the grid active current. The function of the dc-link unbalance control is to balance the voltages $u_{dc\pm}$ across capacitors $C_{dc\pm}$. The function of the current control is to adjust the SC output currents i_{SCabc} (i.e., grid currents i_{Sabc}) to be sinusoidal and balanced. Moreover, k_{pwm}, d_{dq0} and U_{Sdpk} represent the modulator gain, the SC's duty ratio and the maximum value of the grid voltage, respectively.

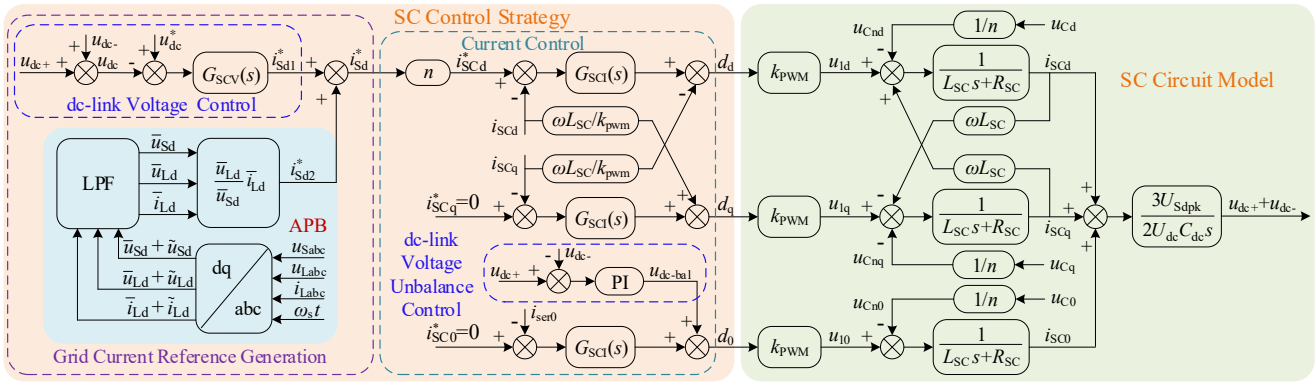

Figure 2. Control block diagram of SC.

In the *dq*0-frame, the grid voltages u_{Sabc}, load voltages u_{Labc} and currents i_{Labc} can be expressed as follows:

$$u_{Sd} = \overline{u}_{Sd} + \widetilde{u}_{Sd}\ u_{Ld} = \overline{u}_{Ld} + \widetilde{u}_{Ld}\ i_{Ld} = \overline{i}_{Ld} + \widetilde{i}_{Ld} \quad (1)$$

where $\overline{u}_{Sd}$, $\overline{u}_{Ld}$ and $\overline{i}_{Ld}$ are the dc components that represent the fundamental components, whereas $\widetilde{u}_{Sd}$, $\widetilde{u}_{Ld}$ and $\widetilde{i}_{Ld}$ are the oscillating components that represent the harmonic components.

Since these oscillation components deteriorate the current reference generation, a second-order low-pass filter (LPF) with the cut-off frequency of 12 Hz is employed to eliminate these components [21], in order to obtain $\overline{u}_{\mathrm{Sd}}$, $\overline{u}_{\mathrm{Ld}}$ and $\overline{i}_{\mathrm{Ld}}$. According to the instantaneous power theory, ignoring the system loss, the relationship between fundamental active powers of the grid side and load side is as follows:

$$\overline{P}_{\mathrm{Sd}} = \overline{u}_{\mathrm{Sd}}\overline{i}_{\mathrm{Sd}} = \overline{u}_{\mathrm{Ld}}\overline{i}_{\mathrm{Ld}} = \overline{P}_{\mathrm{Ld}} \tag{2}$$

From Equation (2), the fundamental active current generated by the APB at the input side of the UPQC can be expressed as follows:

$$i^*_{\mathrm{Sd2}} = \overline{u}_{\mathrm{Ld}}\overline{i}_{\mathrm{Ld}}/\overline{u}_{\mathrm{Sd}} \tag{3}$$

From Equation (3), since i^*_{Sd2} is related to fundamental components (i.e., $\overline{u}_{\mathrm{Sd}}$, $\overline{u}_{\mathrm{Ld}}$ and $\overline{i}_{\mathrm{Ld}}$), the grid only provides active powers for loads.

The total reference i^*_{Sd} is obtained by adding i^*_{Sd1} and i^*_{Sd2}, as follows:

$$i^*_{\mathrm{Sd}} = i^*_{\mathrm{Sd1}} + i^*_{\mathrm{Sd2}} \tag{4}$$

where $i^*_{\mathrm{Sd}}(s) = \mathrm{G_{SCV}}(s)\left[u^*_{\mathrm{Sd}}(s) - u_{\mathrm{dc+}}(s) - u_{\mathrm{dc-}}(s)\right]$.

Since the grid currents are required to be sinusoidal and balanced waveforms, the current references of the *q*- and *0*-axis are set to i^*_{SCq}= 0 and i^*_{SC0}= 0, respectively. Moreover, the dc-link voltage loop is designed as a typical type II control system to obtain the better anti-interference performance. As a result, a type II controller $G_{\mathrm{SCV}}(s) = k_{\mathrm{dc}}(1 + s/\omega_{\mathrm{z}})/(s(1 + s/\omega_{\mathrm{p}}))$ is employed in the dc-link voltage control loop [22], where k_{dc}, ω_{z} and ω_{p} are the controller gain, pole frequency and zero frequency, respectively.

In Figure 2, the reference i^*_{Sd} needs to be multiplied by the transformer Tr turn ratio n to control the SC output currents i_{SCabc}, and thus the grid current $i_{\mathrm{Sd}}(s)$ can be obtained as follows:

$$i_{\mathrm{Sd}}(s) = i_{\mathrm{SCd}}(s)/n = [H_{\mathrm{SCd}}(s)i^*_{\mathrm{SCd}}(s) - u_{\mathrm{Cnd}}(s)/Z_{\mathrm{SCs}}(s)]/n = H_{\mathrm{SCd}}(s)i^*_{\mathrm{Sd}}(s) - u_{\mathrm{Cd}}(s)/Z_{\mathrm{SCp}}(s) \tag{5}$$

where $H_{\mathrm{SCd}}(s) = G_{\mathrm{SCI}}(s)k_{\mathrm{pwm}}/[L_{\mathrm{SC}}\,s + R_{\mathrm{SC}} + G_{\mathrm{SCI}}(s)k_{\mathrm{pwm}}]$, $Z_{\mathrm{SCs}}(s) = [L_{\mathrm{SC}}\,s + R_{\mathrm{SC}} + G_{\mathrm{SCI}}(s)k_{\mathrm{pwm}}]$.

$H_{\mathrm{SCd}}(s)$ is the closed-loop transfer function of the current control loop, $Z_{\mathrm{SCs}}(s)$ and $Z_{\mathrm{SCp}}(s) = n^2 Z_{\mathrm{SCs}}(s)$ are the SC's equivalent impedances on the primary and secondary side of Tr, respectively. $G_{\mathrm{SCI}}(s) = k_{\mathrm{SCip}} + k_{\mathrm{SCii}}/s$ is a proportional-integral (PI) controller, where k_{SCip} and k_{SCii} are the PI controller gains. R_{SC} is the equivalent resistance of the inductor L_{SC}, and $u_{\mathrm{Cnd}}(s) = u_{\mathrm{Cd}}(s)/n$ is the secondary voltage of Tr. The PI controller parameters for the SC can be obtained from the procedure detailed in [23].

From Equation (5), the first term $H_{\mathrm{SCd}}(s)i^*_{\mathrm{Sd}}(s)$ represents the tracking ability of $i_{\mathrm{Sd}}(s)$ to the reference i^*_{Sd}, and the second term $u_{\mathrm{Cd}}(s)/Z_{\mathrm{SCp}}(s)$ represents the disturbance of $u_{\mathrm{Cd}}(s)$ to $i_{\mathrm{Sd}}(s)$. Therefore, the controller $G_{\mathrm{SCI}}(s)$ is required to have a larger gain to reduce the effect of $u_{\mathrm{Cd}}(s)$ on $i_{\mathrm{Sd}}(s)$. According to Equation (5), the SC's Norton impedance model can be obtained in the *d*-axis, as shown in Figure 3. For analysis simplicity, the impedance model on the secondary side of Tr in Figure 3a is equivalent to the primary side in Figure 3b. As a result, the SC is equivalent to a controllable sinusoidal current source $H_{\mathrm{SCd}}(s)i^*_{\mathrm{Sd}}(s)$ in parallel with the equivalent impedance $Z_{\mathrm{SCp}}(s)$. Asides from that, the impedance modeling methods of the *q*- and 0-axis are similar to that of the *d*-axis.

Based on the relationship between $u_{\mathrm{Cd}}(s)$ and $i_{\mathrm{Sd}}(s)$ in Figure 3b, the SC can be equivalent to an output impedance $Z_{\mathrm{SCout}}(s)$, as shown by the dashed line, and its expression is as follows:

$$Z_{\mathrm{SCout}}(s) = \frac{u_{\mathrm{Cd}}(s)}{i_{\mathrm{Sd}}(s)} = \frac{u_{\mathrm{Cd}}(s)}{H_{\mathrm{SCd}}(s)i^*_{\mathrm{Sd}}(s) - u_{\mathrm{Cd}}(s)/Z_{\mathrm{SCp}}(s)} \tag{6}$$

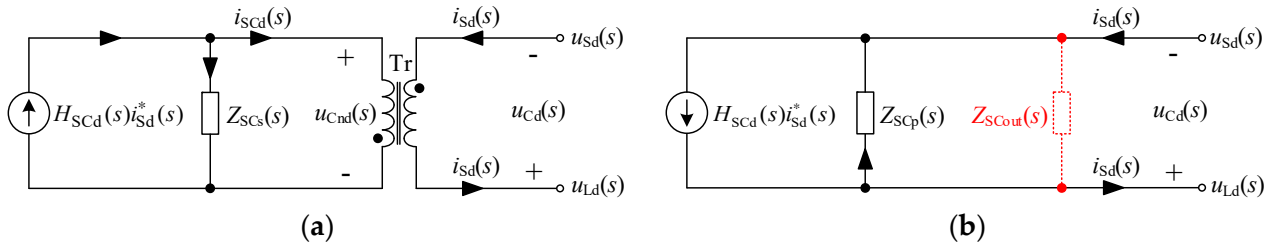

Figure 3. Norton impedance model of SC: (**a**) impedance model at the secondary side; (**b**) impedance model at the primary side.

From Equation (6), $Z_{SCout}(s)$ is related to $H_{SCd}(s)$, $i^*_{Sd}(s)$, $u_{Cd}(s)$ and $Z_{SCp}(s)$. Since $u_{Cd}(s)$ and $i^*_{Sd}(s)$ vary with $u_{Sd}(s)$ and P_{Ld}, $Z_{SCout}(s)$ will be adjusted to control the active power P_{SC} drew or emitted by the SC.

2.2. Parallel Converter Control Strategy and Impedance Model

The PC operates as a controllable sinusoidal voltage source, which is used to control load voltages to be sinusoidal, regulated and balanced. For this purpose, the control strategy of PC is designed, as shown in Figure 4, where the voltage references in the $dq0$-frame are u^*_{Ld}= 311 V and u^*_{Lq}= u^*_{L0} = 0 V, respectively. Considering unbalanced and non-linear loads, the voltage loop controllers $G_{PCV}(s)$ employ the PI + quasi-resonant (QR) controllers, while the current loop controllers $G_{PCI}(s)$ employ the PI controllers.

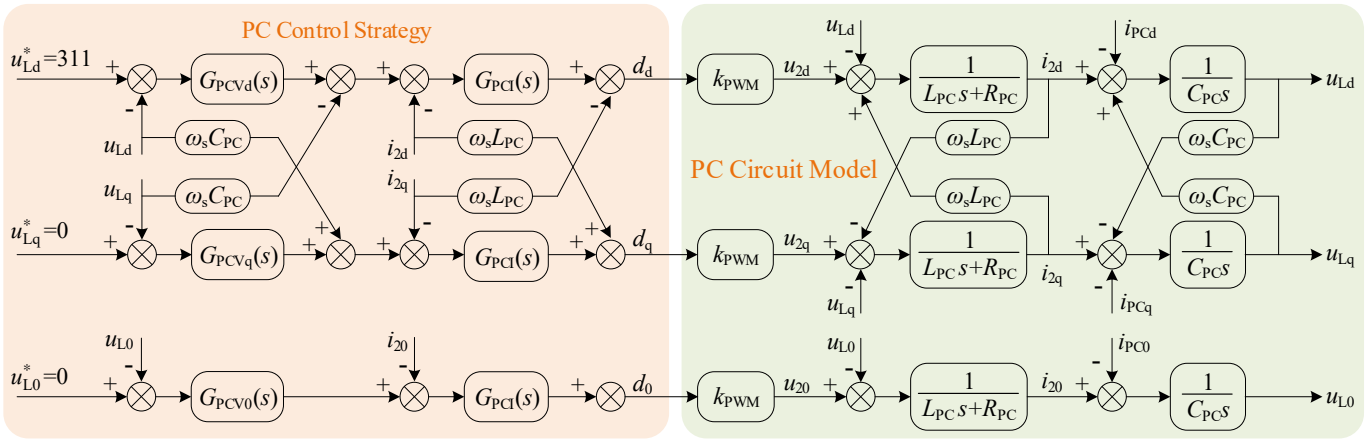

Figure 4. Control block diagram of PC.

From Figure 4, taking the d-axis as an example, the load voltage $u_{Ld}(s)$ can be obtained as follows:

$$u_{Ld}(s) = H_{PCd}(s)u^*_{Ld}(s) - Z_{PC}(s)i_{PCd}(s) \tag{7}$$

where

$$H_{PCd}(s) = \frac{G_{PCVd}(s)G_{PCI}(s)k_{PWM}}{C_{PC}s(L_{PC}s + R_{PC}) + C_{PC}G_{PCI}(s)k_{PWM}s + G_{PCVd}(s)G_{PCI}(s)k_{PWM} + 1}$$

$$Z_{PC}(s) = \frac{L_{PC}s + R_{PC} + G_{PCI}(s)k_{PWM}}{C_{PC}s(L_{PC}s + R_{PC}) + C_{PC}G_{PCI}(s)k_{PWM}s + G_{PCVd}(s)G_{PCI}(s)k_{PWM} + 1}$$

$H_{PCd}(s)$ and $Z_{PC}(s)$ are the closed-loop transfer function and equivalent impedance of the PC, respectively.

To improve the voltage quality of u_L, low-order harmonics need to be suppressed. Specifically, with the increase in the order of harmonics, the harmonic contents will decrease significantly, thus the 3rd, 5th, 7th, 9th, 11th and 13th harmonics will be suppressed as undesirable components. After the $dq0$ coordinate transformation, the 5th and 7th

harmonics as well as the 11th and 13th harmonics are transformed into the 6th and 12th harmonics, respectively, which are reflected on the *d*- and *q*-axis. While, the 3rd and 9th harmonics are directly reflected on the 0-axis. Based on the above analysis, the voltage loop controllers $G_{PCVd,q,0}(s)$ adopt the PI + QR structure, and they can be expressed as follows:

$$\begin{cases} G_{PCVd,q}(s) = k_{PCvp} + \frac{k_{PCvi}}{s} + \sum\limits_{h=6,12} \frac{2k_r\omega_c s}{s^2+2\omega_c s+(h\omega_o)^2} \\ G_{PCV0}(s) = k_{PCvp} + \frac{k_{PCvi}}{s} + \sum\limits_{h=3,9} \frac{2k_r\omega_c s}{s^2+2\omega_c s+(h\omega_o)^2} \end{cases} \quad (8)$$

where k_{PCvp} and k_{PCvi} are the gains of PI controller, and h, k_r, ω_o and ω_c are the harmonic order, resonance coefficient, resonance frequency and cut-off frequency of the QR controller.

It can be noted that the voltage loop PI controllers $k_{PCvp} + k_{PCvi}/s$ are employed to control the dc component of the load voltage generated by the transformation of the ac fundamental components to the *dq0*-frame, while the current loop PI controllers $G_{PCI}(s) = k_{PCip} + k_{PCii}/s$ are employed to control the currents i_{2dq0}. Furthermore, the current and voltage loops are designed as the typical type I and type II control systems, respectively, to achieve the fast dynamic response and good anti-interference performance, and the parameter designs of PI and QR controllers for the PC can be found in [23,24], respectively.

The PC's Thevenin impedance model can be obtained from Equation (7), as shown in Figure 5, that is, the PC is equivalent to a controllable sinusoidal voltage source and an impedance in series. Based on the relationship between load voltage $u_{Ld}(s)$ and the PC's output current $i_{PCd}(s)$, the PC can be equivalent to an output impedance $Z_{PCout}(s)$, as shown by the dashed line, and its expression is as follows:

$$Z_{PCout}(s) = \frac{u_{Ld}(s)}{i_{PCd}(s)} = H_{PCd}(s)\frac{u^*_{Ld}(s)}{i_{PCd}(s)} - Z_{PC}(s) \quad (9)$$

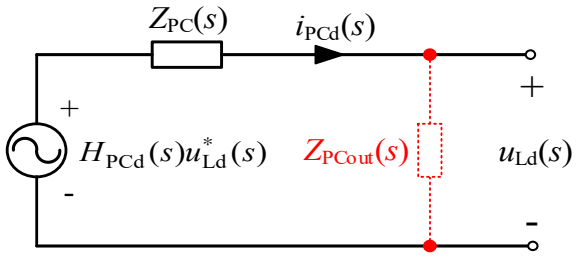

Figure 5. Impedance model of PC.

From Equation (9), $Z_{PCout}(s)$ is not only related to $H_{PCd}(s)$ and $Z_{PC}(s)$, but also related to $i_{PCd}(s)$ that is equal to the difference between $i_{Ld}(s)$ and $i_{Sd}(s)$. When $u_{Sd}(s)$ fluctuates, to balance the active powers between grid side and load side, $i_{Sd}(s)$ will vary with $u_{Sd}(s)$, thus $i_{PCd}(s)$ is determined by $u_{Sd}(s)$. As a result, the changes of $u_{Sd}(s)$ will lead to the changes of $Z_{PCout}(s)$, so as to control the active power $P_{PC}(s)$ drew or emitted by the PC.

2.3. Equivalent Impedance Model for UPQC

The UPQC equivalent impedance model can be obtained from Equations (5) and (7), as shown in Figure 6a. To simplify the analysis, a simplified impedance model can be obtained from Equations (6) and (9), as shown in Figure 6b, where $Z_S(s)$ and $Z_{out}(s)$ are the input and output equivalent impedances, and can be expressed as follows:

$$Z_S(s) = u_S(s)/i_S(s) \quad (10)$$

$$Z_{out}(s) = [Z_S(s) + Z_{SCout}(s)]//Z_{PCout}(s) \quad (11)$$

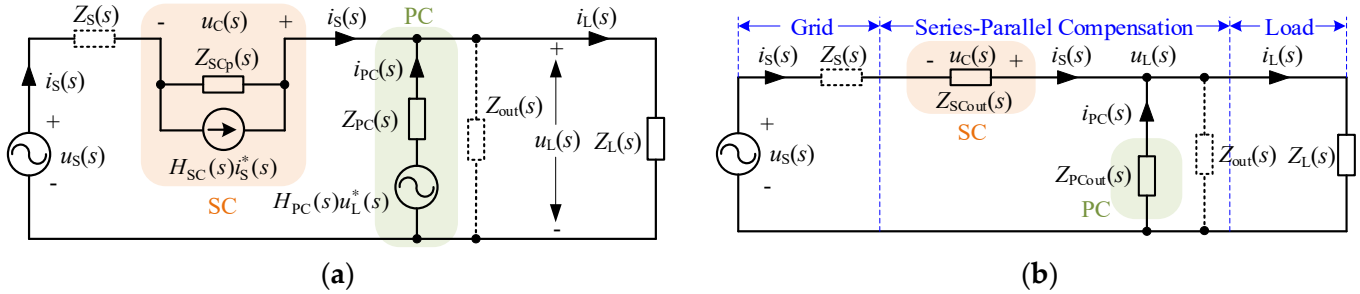

Figure 6. UPQC impedance model: (**a**) equivalent model; (**b**) simplified model.

After the impedance model is established, the matching relationships among node impedances will be studied to analyze the operation principle of UPQC power flow, and the system control parameters are shown in Table 2.

Table 2. UPQC control parameters.

SC	Current controller $G_{SCI}(s)$	$k_{SCip} = 6.43$ $k_{SCii} = 8.19\times10^3$
	Voltage controller $G_{SCV}(s)$	$k_{dc} = 265$ $\omega_z = 8.42$ rad/s $\omega_p = 117$ rad/s
PC	Current controller $G_{PCI}(s)$	$k_{PCip} = 0.96$ $k_{PCii} = 319$
	Voltage controller $G_{PCV}(s)$	$k_{PCvp} = 0.16$ $k_{PCvi} = 77.51$ $k_r = 50$ $\omega_c = 5$ rad/s $\omega_o = 100$ rad/s

3. Power Flow and Impedance Matching

The concept of impedance matching is involved in the UPQC's impedance model to discuss the operation principle of power flows in this section. To simplify the analysis for the power flow and impedance matching, supposing that: (a) u_{Sabc} are pure sinusoidal, and their root-mean-square (RMS) values U_{Sabc} are equal to U_S; (b) the dc-link voltage is stable and the UPQC's loss is zero.

The RMS values of load voltages U_{Labc} are equal to U_L under the control of PC, and the variation degree of grid voltage k_u can be defined as follows:

$$k_u = (U_S - U_L)/U_L \tag{12}$$

From Equation (12), this value of k_u is determined by U_S. On the basis of the variation degree k_u, the theoretical analysis process can be carried out from the following three cases: (1) Case A: $U_S = U_L$, $k_u = 0$; (2) Case B: $U_S > U_L$, $k_u > 0$; (3) Case C: $U_S < U_L$, $k_u < 0$.

3.1. Impedance Matching-Based Power Flow Analysis in Case A

In Case A (i.e., $U_S = U_L$, $k_u = 0$), the grid provides all the active power for the load through path 1 (defined as: from the grid to the load through the transformer), and Figure 7 shows the operation principle of the UPQC in Case A.

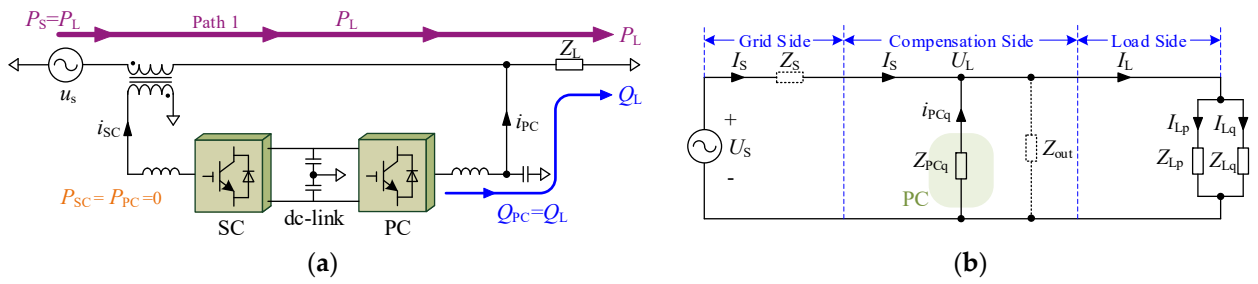

Figure 7. Operation principle in Case A: (**a**) power flows principle; (**b**) impedance matching principle.

3.1.1. Power Flow

In Figure 7a, Z_L is a resistive-inductive (*R-L*) load impedance consisting of Z_{Lp} and Z_{Lq}, and thus the load current i_L consists of the active and reactive currents i_{Lp} and i_{Lq}. Thus, the active and reactive powers of load impedance P_L and Q_L can be expressed as follows:

$$\begin{cases} P_L = U_L I_L \cos\varphi_L = U_L I_{Lp} \\ Q_L = U_L I_L \sin\varphi_L = U_L I_{Lq} \end{cases} \tag{13}$$

where the subscripts p and q represent the active and reactive components, respectively, φ_L is the load power factor angle.

In Case A, the electrical quantities of UPQC system meet the following relationships:

$$\begin{cases} I_S = I_{Lp}, I_{PCp} = 0, I_{PCq} = I_{Lq}, U_C = 0 \\ P_S = P_L, Q_{PC} = Q_L, P_{SC} = P_{PC} = 0, Q_{SC} = 0 \end{cases} \tag{14}$$

From Equation (14), both U_C and I_{PCp} are zero, thus $P_{SC} = P_{PC} = 0$, meaning that there is no active power transmission between SC and PC. Additionally, the grid and the PC provide all active and reactive power for the load, respectively.

3.1.2. Impedance Matching

In Figure 7b, the input equivalent impedance Z_S can be calculated as follows:

$$Z_S = U_S / I_S = U_L / I_{Lp} = Z_{Lp} \tag{15}$$

From Equation (15), due to $Z_S = Z_{Lp}$, the input active power P_S is equal to the load active power P_L.

Not only that, due to $U_C = 0$ and $I_{PCp} = 0$, the SC's output impedance Z_{SCout} is equal to zero, while the PC's output resistive impedance Z_{PCp} is infinite. This means that the SC and PC do not get involved in the resistive impedance matching.

Since the PC compensates the all reactive power for the load, the PC's inductive impedance Z_{PCq} can be expressed as follows:

$$Z_{PCq} = U_L / I_{PCq} = U_L / I_{Lq} = Z_{Lq} \tag{16}$$

The output equivalent impedance Z_{out} can be expressed as follows:

$$Z_{out} = Z_S // Z_{PCq} = Z_{Lp} // Z_{Lq} = Z_L \tag{17}$$

From the above analysis, in Case A, only the PC is involved in the inductive impedance matching. Furthermore, Z_S, Z_{PCq} and Z_{out} contain the factor Z_L (Z_{Lp} or Z_{Lq}), which indicates that these node impedances are adjusted only depending on the load.

3.2. Impedance Matching-Based Power Flow Analysis in Case B

In Case B (i.e., $U_S > U_L$, $k_u > 0$), in addition to path 1, the grid provides the active power for the load through path 2 (defined as: from the SC to the PC or from the PC to the SC). To this end, the node impedances will be matched again, owing to $U_S > U_L$, aiming to balance the power flows. To analyze the operation principle more clearly, an M point is marked behind the transformer, and the operation principle is shown in Figure 8.

3.2.1. Power Flow

As U_S increases (i.e., $U_S = (1 + k_u)U_L$), I_S will be reduced to ensure $P_S = P_L$, according to Equations (3) and (12), I_S can be expressed as follows:

$$I_S = I_{Lp} / (1 + k_u) \tag{18}$$

From Equation (18), I_S is reduced by $(1 + k_u)$ times.

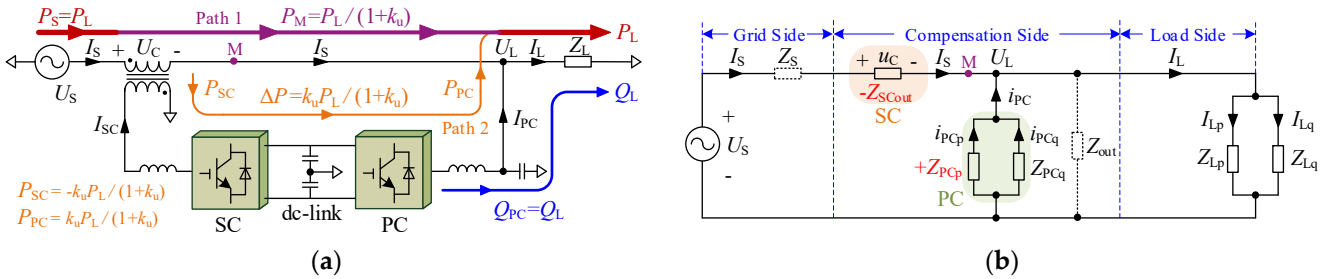

Figure 8. Operation principle in Case B: (**a**) power flows principle; (**b**) impedance matching principle.

The increase in U_S results in a voltage difference between grid side and load side, which is added the transformer Tr. Thus, the voltage U_C across Tr can be expressed as follows:

$$U_C = U_L - U_S = -k_u U_L \tag{19}$$

Combining Equations (18) and (19), the SC's active power P_{SC} can be obtained as follows:

$$P_{SC} = U_C I_S = -k_u P_L/(1+k_u) \tag{20}$$

From Equation (20), P_{SC} is negative due to U_C, which indicates that the SC draws the active power from the grid.

After the transformer compensation (i.e., M point), the voltage of path 1 is U_L, while the I_S remains the same, so the active power of path 1 can be expressed as follows:

$$P_M = U_L I_S = P_L/(1+k_u) \tag{21}$$

It can be seen from Equation (21) that P_M is less than P_L, meaning that path 1 cannot meet the power requirements of the load. For this reason, the PC provides the load with the active power drew by the SC, as can be seen in path 2.

The PC compensates both the active and reactive powers and its output current I_{PC} can be expressed as follows:

$$I_{PC} = I_{PCp} + I_{PCq} = (I_{Lp} - I_S) + I_{PCq} = \frac{k_u}{1+k_u} I_{Lp} + I_{Lq} \tag{22}$$

Combining U_L and I_{PCp}, the PC's output active power P_{PC} can be obtained as follows:

$$P_{PC} = U_L I_{PCp} = k_u P_L/(1+k_u) \tag{23}$$

It can be seen from Equation (23) that P_{PC} is positive, which indicates that the PC emits the active power.

The energy ΔP transferred between SC and PC is as follows:

$$\Delta P = |P_{SC}| = P_{PC} \tag{24}$$

In terms of reactive power, the phase angle difference between voltage U_C across the transformer and grid current I_S is π, which results in the reactive power Q_{SC} of SC as zero. While the PC provides all the reactive current and power for the load, so the reactive power Q_{PC} output by the PC is equal to Q_L.

3.2.2. Impedance Matching

Compared with Case A, node impedances Z_S, Z_{SCout} and Z_{PCout} are matched to make Z_{out} equal to Z_L in Case B.

According to Equations (10) and (18), Z_S can be calculated as follows:

$$Z_S = U_S/I_S = (1+k_u)^2 Z_{Lp} \tag{25}$$

From Equation (25), Z_S is $(1 + k_u)^2$ times Z_{Lp} due to $U_S > U_L$.

The SC's output impedance Z_{SCout} can be calculated as follows:

$$Z_{SCout} = U_C / I_S = -k_u(1 + k_u)Z_{Lp} \tag{26}$$

From Equation (26), the direction of Z_{SCout} is determined by U_C, resulting in Z_{SCout} being negative, which indicates that the SC operates in a rectified state to draw the active power.

The impedance Z_M at M-point can be calculated as follows:

$$Z_M = Z_S + Z_{SCout} = U_L / I_S = (1 + k_u)Z_{Lp} \tag{27}$$

From Equation (27), due to $Z_M \neq Z_{LP}$, the active powers of UPQC system cannot be balanced if the impedance matching behavior is performed by the SC alone. For this reason, the PC is required to participate in the impedance matching, and the PC's output impedance Z_{PCout} can be calculated as follows:

$$Z_{PCout} = \frac{U_L}{I_{PC}} = Z_{PCp} // Z_{PCq} = \left(\frac{1 + k_u}{k_u} Z_{Lp}\right) // Z_{Lq} \tag{28}$$

From Equation (28), the direction of the resistive impedance Z_{PCp} is determined by I_{PCp}, resulting in Z_{PCp} being positive, which indicates that the PC operates in an inverter state to provide the load with the active power drawn by the SC. Moreover, the inductive load impedance Z_{Lq} is only compensated by the PC (i.e., $Z_{PCq} = Z_{Lq}$).

Comparing Equations (20) and (23) with Equations (26) and (28), it can be found that the active power transmitted by two converters is the same, but their output impedances are different, and the difference between Z_{SCout} and Z_{PCout} is k_u^2 times. This indicates that the range of impedance regulated by the PC is wider than that regulated by the SC under the condition of the same transmission power.

According to Equations (25), (26) and (28), Z_{out} can be expressed as follows:

$$Z_{out} = Z_M // Z_{PCout} = Z_L \tag{29}$$

From Equation (29), after the node impedances are dynamically matched, Z_{out} is equal to Z_L, which achieves the impedance balance of the UPQC.

In Case B, all node impedances have two factors k_u and Z_{Lp}, which means that these impedances are adjusted depending on the grid voltage and the load, and thus achieving $Z_{out} = Z_L$. In consequence, when the node impedances reach an equilibrium state again, the power flows of the system will be accompanied by stability and balance.

3.3. Impedance Matching-Based Power Flow Analysis in Case C

Figure 9 shows the operation principle in Case C (i.e., $U_S < U_L$, $k_u < 0$), the analysis process in Case C is like that in Case B, and will not be repeated here. The difference is that path 1 will generate the excess active power due to the increase in grid current. To balance the system energy, the SC and PC output a positive and negative impedance, respectively, which causes the PC to draw this excess energy and the SC to return it to path 1 via path 2.

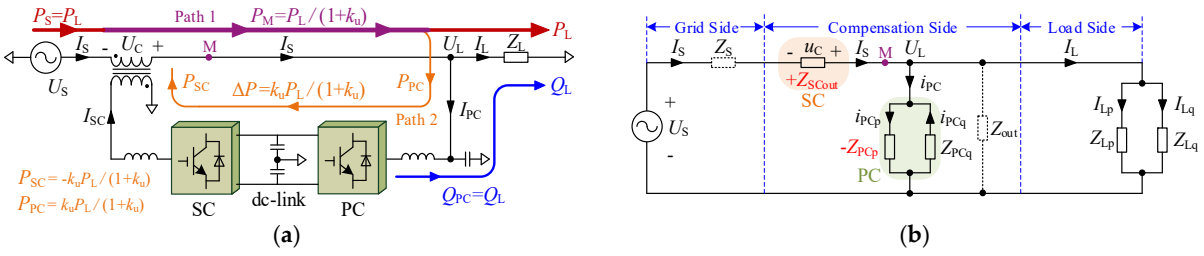

Figure 9. Operation principle in Case C: (**a**) power flows principle; (**b**) impedance matching principle.

It should be noted that due to the definition of k_u in Equation (14), the expressions of voltage (U_C), currents (I_S, I_{PC}), active powers (P_{SC}, P_M, P_{PC}, ΔP), reactive powers (Q_{SC}, Q_{PC}) and node impedances (Z_S, Z_{SCout}, Z_M, Z_{PCout}, Z_{out}) in Case C are the same as those in Case B. However, due to $k_u < 0$ in Case C, the directions of U_C, I_{PCp}, P_{SC}, P_{PC}, ΔP, Z_{SCout} and Z_{PCp} are opposite to that in Case B.

4. Case Analysis

To investigate the correctness and adaptability of the above theoretical analysis, this section will quantitatively conduct some case analysis on the matching relationships between active power flows and node impedances.

The case analysis conditions are as follows:

(1) The 9.8 kW × 3 three-phase balanced resistive loads are taken as an example to analyze the power flow and impedance matching.

(2) For purposes of analysis, it is supposed that the UPQC is lossless and the dc-link voltage is controlled to be stable.

(3) Referring to IEC 60038-2009, the variation ranges of U_S are not more than ±10%. To prove the operation ability of the UPQC to grid voltage fluctuations, the fluctuation range is set to ±15% in this paper. The upper and lower limits of U_S are taken as the analysis conditions, the three cases in the previous section are redefined as follows:

Case A: U_S = 220 V, k_u = 0;

Case B: U_S = 253 V, k_u = +15%;

Case C: U_S = 187 V, k_u = −15%.

According to Section 3, Figure 10 shows the quantitative matching relationships among the active powers, node impedances and grid voltages in the three redefined cases. From Figure 10a,b, P_{Sabc} are always equal to P_{Labc}, while Z_{Sabc} and Z_{Labc} are only equal at 220 V. Furthermore, P_{Mabc} and P_{SCabc} keep decreasing, while P_{PCabc} keep increasing, where P_{SCabc} and P_{PCabc} always remain the same amplitude and the opposite direction, indicating that one converter operates in rectifier state and the other one operates in inverter state. Z_{Sabc} and Z_{Mabc} always keep increasing, while Z_{outabc} and Z_{Labc} remain unchanged and always equal. Additionally, $Z_{SCoutabc}$ continuously decreases, and they are zero only at U_{Sabc} = 220 V, which is in line with the series characteristics of the SC.

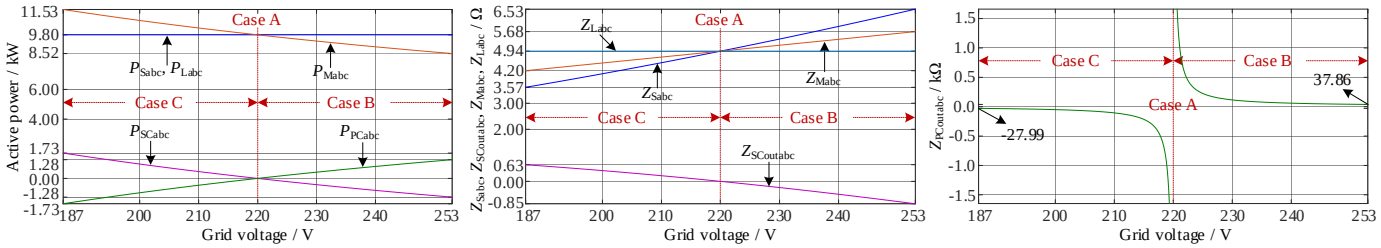

(**a**) (**b**) (**c**)

Figure 10. Power flows and node impedances in Case A–C: (**a**) P_{Sabc}, P_{SCabc}, P_{Mabc}, P_{PCabc} and P_{Labc}; (**b**) Z_{Sabc}, $Z_{SCoutabc}$, Z_{Mabc} and Z_{Labc}; (**c**) $Z_{PCoutabc}$.

From Figure 10c, $Z_{PCoutabc}$ are divided into two parts. The closer the two parts are to 220 V, the greater $Z_{PCoutabc}$, and their impedances are infinite at U_{Sabc} = 220 V, which is in line with the parallel characteristics of the PC.

For comparison with the experimental results in the next section, the theoretical calculation results of voltages, currents, active powers and node impedances in Case A–C are shown in Table 3.

From Table 3, the difference ΔP between P_{Mabc} and P_{Labc} is compensated by the two converters, i.e., $|\Delta P| = |P_{\mathrm{Mabc}} - P_{\mathrm{Labc}}| = |P_{\mathrm{SCabc}}| = |P_{\mathrm{PCabc}}|$. Aside from that, the fluctuation rates of U_{Sabc} are +15% and −15% in Case B and C, respectively, whereas the variation rates of I_{Sabc}, P_{SCabc} and P_{PCabc} are 13.04% and 17.65% from Equations (18), (20) and (23).

Table 3. Theoretical calculation results of voltages (RMS), currents (RMS), active powers and node impedances.

Quantity	Case A	Case B	Case C	Quantity	Case A	Case B	Case C
U_{Sabc}/V	220	253	187	P_{PCabc}/kW	0	1.28	−1.73
U_{Labc}/V	220	220	220	P_{Labc}/kW	9.8	9.8	9.8
U_{Cabc}/V	0	−33	33	Z_{Sabc}/Ω	4.94	6.53	3.57
I_{Labc}/V	44.54	44.54	44.54	Z_{SCoutabc}/Ω	0	−0.85	0.63
I_{Sabc}/V	44.54	38.73	52.41	Z_{Mabc}/Ω	4.94	5.68	4.20
I_{PCabc}/V	0	5.81	−7.86	Z_{PCoutabc}/Ω	∞	37.86	−27.99
P_{Sabc}/kW	9.8	9.8	9.8	Z_{outabc}/Ω	4.94	4.94	4.94
P_{SCabc}/kW	0	−1.28	1.73	Z_{Labc}/Ω	4.94	4.94	4.94
P_{Mabc}/kW	9.8	8.52	11.53				

5. Experimental Validation

In order to verify the correctness of power flow analysis based on impedance matching, the UPQC hardware prototype system has been developed to perform the relevant experiments, as shown in Figure 11. The developed control algorithms have been embedded into two DSPs (TMS320F28335), and parameters used for the experimentation are shown in Tables 1 and 2.

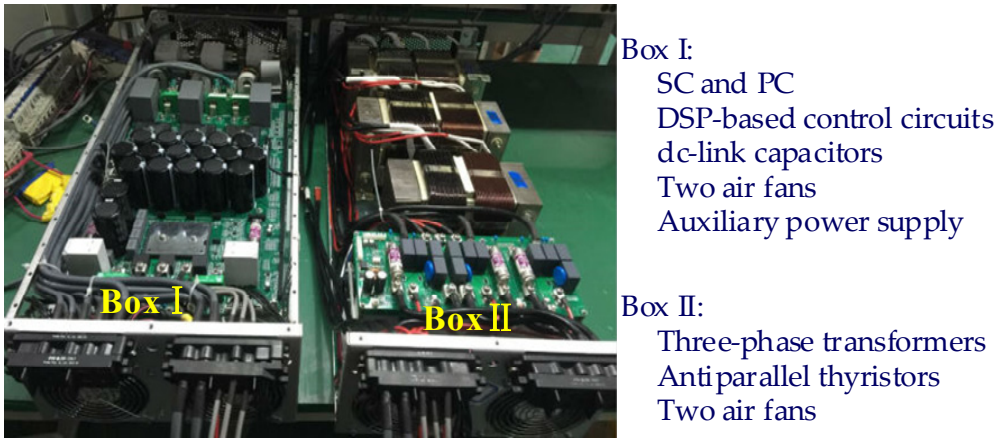

Figure 11. UPQC laboratory prototype.

It is important to note that the UPQC draws loss currents from the grid to compensate for its system losses during the implementation of experiments. Hence, the influence of loss currents needs to be addressed for the evaluation of node impedances. These losses are consumed in three-phase transformers, a 240 W auxiliary power supply, four 24 W air fans and other losses. Figure 12 shows loss currents i_{Sabc} drawn by the UPQC from the grid with Case A and no-load, in which their RMS values are 2.09 A, 2.18 A and 1.97 A, respectively.

Figure 13 shows the experimental results of the power flow and impedance matching in Case A. The grid voltages u_{Sabc} (221 V, 221 V, 221 V) and the load voltages u_{Labc} (221 V, 221 V, 220 V) are in phase and equal to each other, indicating that the voltages u_{Cabc} across $\mathrm{Tr}_{\mathrm{abc}}$ do not contain the differences between u_{Sabc} and u_{Labc}, as shown in Figure 13a,d. The grid currents i_{Sabc} (46.6 A, 46.8 A, 46.7 A) are in phase with u_{Sabc}, thus gaining unity power factor at the grid side. As i_{Sabc} contain loss currents, they are larger than the load currents i_{Labc} (44.4 A, 44.5 A, 44.7 A), as shown in Figure 13b,e. In fact, because of the presence of

L_s and transformer leakage inductance, the smaller compensation voltages (6.22 V, 5.96 V, 6.15 V) are added to Tr_{abc} in Figure 13c. The PC draws the loss currents (3.21 A, 3.29 A, 3.23 A) to maintain the stability of the dc-link voltage in Figure 13f.

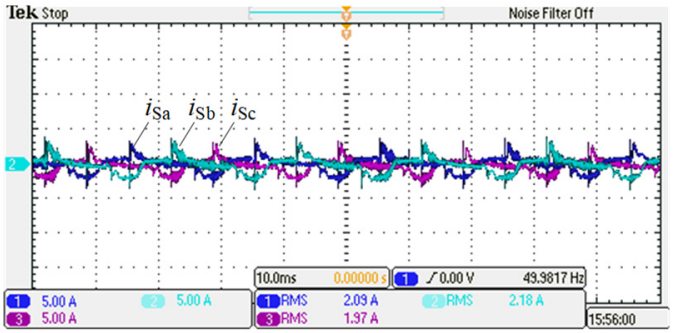

Figure 12. Loss currents i_{Sabc} with Case A and no-load (10 A/div).

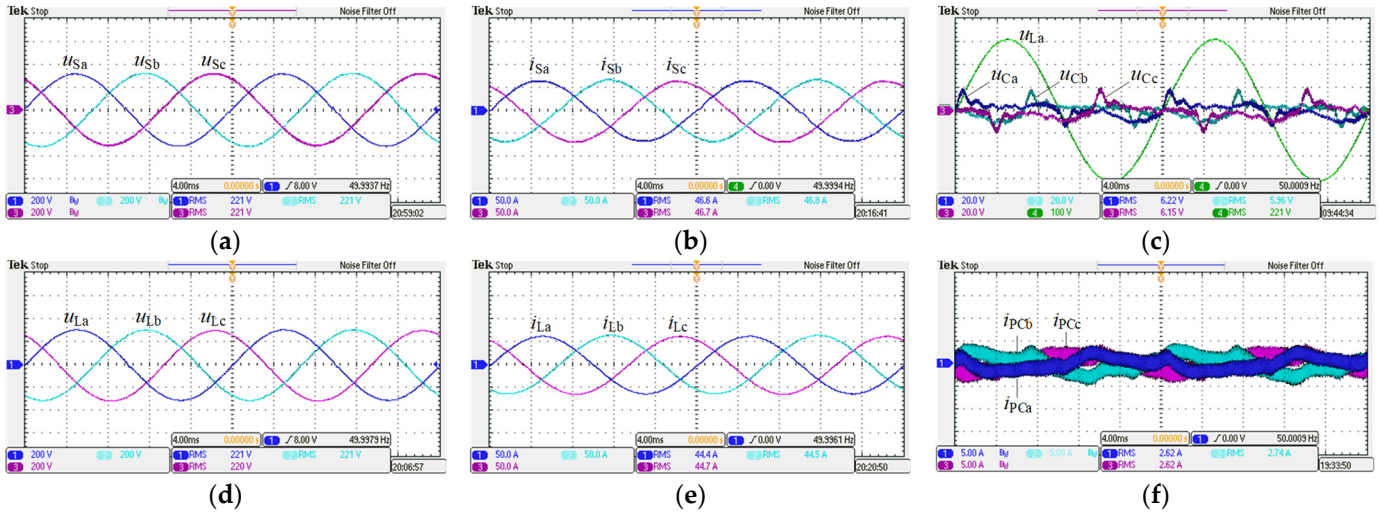

Figure 13. Experimental results of the power flow and impedance matching in Case A (time: 4 ms/div): (**a**) u_{Sabc} (200 V/div); (**b**) i_{Sabc} (50 A/div); (**c**) u_{Cabc} (20 V/div, 100 V/div); (**d**) u_{Labc} (200 V/div); (**e**) i_{Labc} (50 A/div); (**f**) i_{PCabc} (10 A/div).

Figure 14 shows the experimental results of the power flow and impedance matching in Case B. u_{Sabc} swell 15% (253 V, 254 V, 252 V) in Figure 14a, but u_{Labc} are not affected by u_{Sabc} under the PC's control, as shown in Figure 14d. To balance the active power between grid side and load side, i_{Sabc} (40.4 A, 40.8 A, 40.2 A) are reduced accordingly, even below i_{Labc}, as shown in Figure 14b,e. From Figure 14a,b, i_{Sabc} and u_{Sabc} are still in phase. Unlike Case A, u_{Cabc} withstand the reverse voltages (i.e., the voltage differences between u_{Sabc} and u_{Labc}) to compensate for the swell part of u_{Sabc} in Figure 14c. As a result, the directions of u_{Cabc} are opposite to that of i_{Sabc}, which indicates that the SC operates in a rectifier state to draw the active powers from the grid. In Figure 14f, the PC's output currents i_{PCabc} are in phase with u_{Labc}, indicating that the PC operates in an inverter state to transmit the active powers to the loads.

Figure 15 shows the experimental results of Case C, and its analysis process is similar to that of Case B, thus will not be repeated.

Based on the experimental results from Figures 13–15, the actual values of the voltages, currents, active powers, and node impedances are listed in Table 4. As mentioned earlier, the influences of the loss currents in Figure 12 on i_{Sabc} and i_{PCabc} should be considered for experimental results in Table 4. To be more specific, taking Case B as an example to calculate the loss currents and grid currents is as follows: in terms of loss currents, A-phase is 1.82 A (221 × 2.09/253), B-phase is 1.91 A (221 × 2.18/252), and C-phase

is 1.71 A (220 × 1.97/254). In terms of grid currents, combined with the calculated loss currents, the actual RMS values of i_{Sabc} are 38.58 A, 38.89 A and 38.49 A, respectively. From Table 4, experimental results are relatively close to the theoretical calculation results in Table 3, which endorse the correctness of power flow analysis based on the impedance matching method.

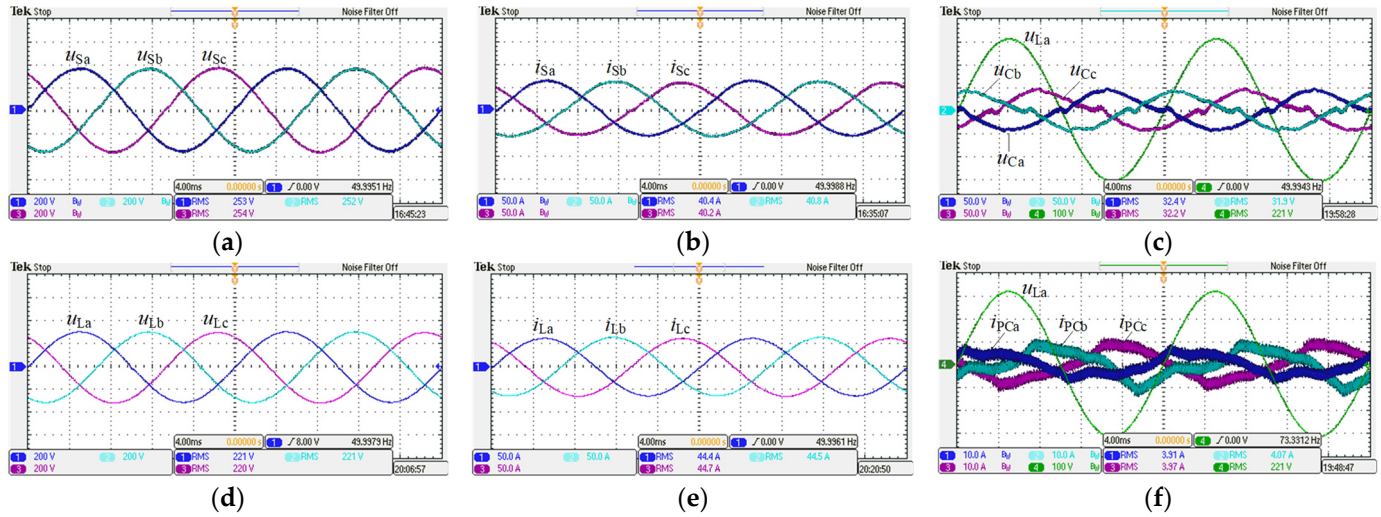

Figure 14. Experimental results of the power flow and impedance matching in Case B (time: 4 ms/div): (**a**) u_{Sabc} (200 V/div); (**b**) i_{Sabc} (50 A/div); (**c**) u_{Cabc} (50 V/div, 100 V/div); (**d**) u_{Labc} (200 V/div); (**e**) i_{Labc} (50 A/div); (**f**) i_{PCabc} (10 A/div, 100 V/div).

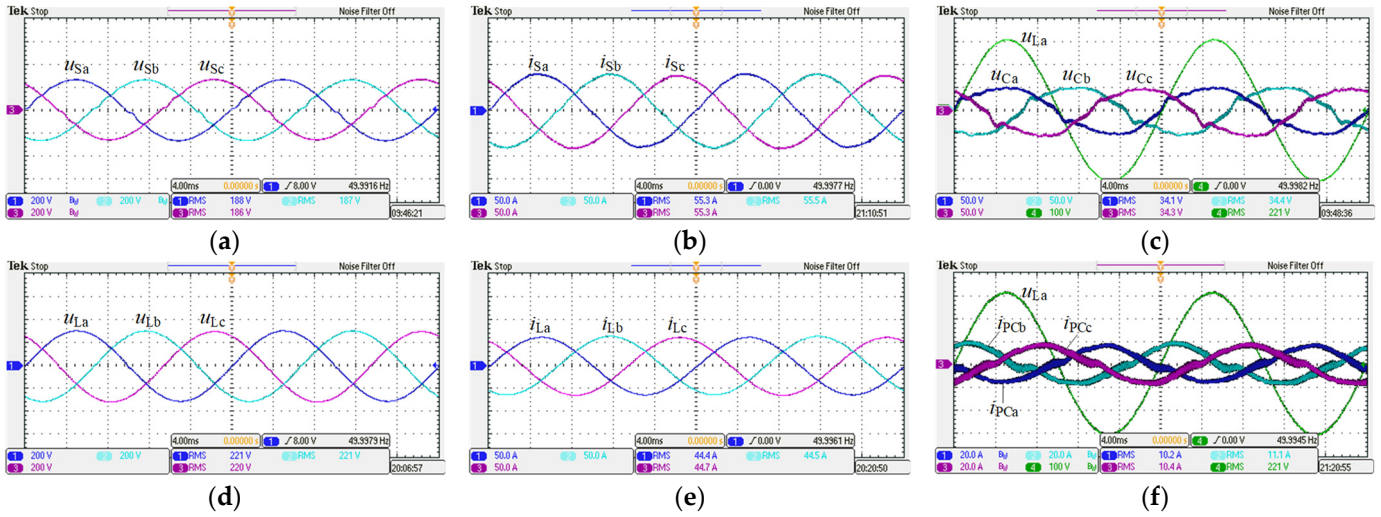

Figure 15. Experimental results of the power flow and impedance matching in Case C (time: 4 ms/div): (**a**) u_{Sabc} (200 V/div); (**b**) i_{Sabc} (50 A/div); (**c**) u_{Cabc} (50 V/div, 100 V/div); (**d**) u_{Labc} (200 V/div); (**e**) i_{Labc} (50 A/div); (**f**) i_{PCabc} (20 A/div, 100 V/div).

Table 4. Experimental results of voltages (RMS), currents (RMS), active powers and node impedances.

Quantity	Case A	Case B	Case C	Quantity	Case A	Case B	Case C
U_{Sa}/V	221	253	188	P_{Mc}/kW	9.84	8.47	11.65
U_{Sb}/V	221	252	187	P_{PCa}/kW	0.25	1.27	−1.71
U_{Sc}/V	221	254	186	P_{PCb}/kW	0.25	1.32	−1.77
I_{Sa}/A	44.51	38.58	52.84	P_{PCc}/kW	0.28	1.25	−1.78
I_{Sb}/A	44.62	38.89	52.92	P_{La}/kW	9.81	9.81	9.81
I_{Sc}/A	44.73	38.49	52.97	P_{Lb}/kW	9.83	9.83	9.83

Table 4. *Cont.*

Quantity	Case A	Case B	Case C	Quantity	Case A	Case B	Case C
U_{Ca}/V	6.22	−32.4	34.1	P_{Lc}/kW	9.83	9.83	9.83
U_{Cb}/V	5.96	−31.9	34.4	Z_{Sa}/Ω	4.97	6.56	3.56
U_{Cc}/V	6.15	−32.2	34.3	Z_{Sb}/Ω	4.95	6.48	3.53
I_{PCa}/A	1.12	5.73	−7.74	Z_{Sc}/Ω	4.94	6.60	3.51
I_{PCb}/A	1.11	5.98	−8.02	Z_{SCouta}/Ω	0.14	−0.84	0.65
I_{PCc}/A	1.26	5.68	−8.07	Z_{SCoutb}/Ω	0.13	−0.82	0.65
U_{La}/V	221	221	221	Z_{SCoutc}/Ω	0.14	−0.83	0.64
U_{Lb}/V	221	221	221	Z_{Ma}/Ω	4.97	5.73	4.18
U_{Lc}/V	220	220	220	Z_{Mb}/Ω	4.95	5.68	4.18
I_{La}/A	44.4	44.4	44.4	Z_{Mc}/Ω	4.92	5.71	4.15
I_{Lb}/A	44.5	44.5	44.5	Z_{PCouta}/Ω	416.98	38.57	−28.55
I_{Lc}/A	44.7	44.7	44.7	Z_{PCoutb}/Ω	394.64	36.97	−27.56
P_{Sa}/kW	9.84	9.76	9.93	Z_{PCoutc}/Ω	338.46	38.73	−27.26
P_{Sb}/kW	9.86	9.80	9.89	Z_{outa}/Ω	4.98	4.98	4.94
P_{Sc}/kW	9.89	9.78	9.85	Z_{outb}/Ω	4.95	4.91	4.93
P_{SCa}/kW	0.28	−1.25	1.80	Z_{outc}/Ω	4.93	5.02	4.89
P_{SCb}/kW	0.27	−1.24	1.82	Z_{La}/Ω	4.98	4.98	4.98
P_{SCc}/kW	0.28	−1.24	1.82	Z_{Lb}/Ω	4.97	4.97	4.97
P_{Ma}/kW	9.84	8.53	11.68	Z_{Lc}/Ω	4.92	4.92	4.92
P_{Mb}/kW	9.86	8.59	11.70				

6. Conclusions

In this paper, the impedance matching method is introduced to discuss the operation principle for the UPQC in three-phase four-wire systems. On the basis of the designed control strategies, the UPQC is equivalent to an adjustable impedance model with five nodes, and then the corresponding relationships between power flows and node impedances changing with grid voltages are analyzed from this model. When grid voltages change, the original matching state of node impedances is broken, and then all node impedances are dynamically matched to achieve the impedance and power balances of the UPQC. Experimental results from the hardware prototype system have validated the correctness of power flow analysis based on the impedance matching method, and some conclusions can be drawn as follows:

(1) In Case A, the input equivalent impedances are equal to the load impedances, while the SC's output impedances are almost zero, and the PC's output resistive impedances are large, so both converters do not participate in the power transmission.
(2) In Case B, both the input equivalent impedances and the impedances at M-point are increased; moreover the SC outputs the negative impedances and draws the active powers, while the PC outputs the positive impedances and emits the active powers.
(3) The impedance matching relationships in Case C are opposite to that in Case B.
(4) No matter what grid voltages change, system node impedances are dynamically matched to ensure that the output equivalent impedances are always equal to the load impedances.

Author Contributions: Conceptualization, X.Z. and X.C.; methodology, X.Z. and X.G.; software, A.W. and X.C.; validation, X.Z., X.C. and X.G.; formal analysis, A.W. and X.W.; investigation, X.C. and X.W.; resources, X.Z. and C.Z.; data curation, A.W. and X.C.; writing—original draft preparation, X.Z.; writing—review and editing, X.Z., A.W. and X.G.; visualization, X.Z.; supervision, X.G. All authors have read and agreed to the published version of the manuscript.

Funding: This work was supported in part by the National Natural Science Foundation of China under Grant 62003297 and 52077191, and in part by the Natural Science Foundation of Hebei Province of China under Grant E2020203192 and E2018203152.

Institutional Review Board Statement: Not applicable.

Informed Consent Statement: Not applicable.

Data Availability Statement: Not applicable.

Conflicts of Interest: The authors declare no conflict of interest.

References

1. Zeraati, M.; Golshan, M.; Guerrero, J.M. Voltage quality improvement in low voltage distribution networks using reactive power capability of single-phase PV inverters. *IEEE Trans. Smart Grid* **2019**, *10*, 5057–5065. [CrossRef]
2. Parvez, I.; Aghili, M.; Sarwat, A.I.; Rahman, S.; Alam, F. Online power quality disturbance detection by support vector machine in smart meter. *J. Mod. Power Syst. Clean Energy* **2019**, *7*, 1328–1339. [CrossRef]
3. Yang, Y.; Xiao, X.; Guo, S.; Gao, Y.; Yuan, C.; Yang, W. Energy storage characteristic analysis of voltage sags compensation for UPQC based on MMC for medium voltage distribution system. *Energies* **2018**, *11*, 923. [CrossRef]
4. Andrzej, S. The unified power quality conditioner control method based on the equivalent conductance signals of the compensated Load. *Energies* **2020**, *13*, 6298.
5. Yang, D.; Ma, Z.; Gao, X.; Ma, Z.; Cui, E. Control strategy of intergrated photovoltaic-UPQC system for DC-bus voltage stability and voltage sags compensation. *Energies* **2019**, *12*, 4009. [CrossRef]
6. Campanhol, L.B.G.; Silva, S.A.O.; Oliveira, A.A.; Bacon, V.D. Power flow and stability analyses of a multifunctional distributed generation system integrating a photovoltaic system with unified power quality conditioner. *IEEE Trans. Power Electron.* **2019**, *34*, 6241–6256. [CrossRef]
7. Lee, W.C.D.; Lee, M.; Lee, T.K. New control scheme for a unified power-quality compensator-Q with minimum active power injection. *IEEE Trans. Power Del.* **2010**, *25*, 1068–1076. [CrossRef]
8. Xu, Y.; Xiao, X.; Sun, Y.; Long, Y. Voltage sag compensation strategy for unified power quality conditioner with simultaneous reactive power injection. *J. Mod. Power Syst. Clean Energy* **2016**, *4*, 113–122. [CrossRef]
9. Xia, M.; Li, X. Design and Implementation of a High Quality Power Supply Scheme for Distributed Generation in a Micro-Grid. *Energies* **2013**, *6*, 4924–4944. [CrossRef]
10. Kumar, G.S.; Kumar, B.K.; Mishra, M.K. Mitigation of voltage sags with phase jumps by UPQC with PSO-based ANFIS. *IEEE Trans. Power Del.* **2011**, *26*, 2761–2773. [CrossRef]
11. Devassy, S.; Singh, B. Modified pq-theory-based control of solar-PV-integrated UPQC-S. *IEEE Trans. Ind. Appl.* **2017**, *53*, 5031–5040. [CrossRef]
12. Khadkikar, V.; Chandra, A. UPQC-S: A novel concept of simultaneous voltage sag/swell and load reactive power compensations utilizing series inverter of UPQC. *IEEE Trans. Power Electron.* **2011**, *26*, 2414–2425. [CrossRef]
13. He, Y.; Chung, H.S.; Lai, C.; Zhang, X.; Wu, W. Active cancelation of equivalent grid impedance for improving stability and injected power quality of grid-connected inverter under variable grid condition. *IEEE Trans. Power Electron.* **2018**, *33*, 9387–9398. [CrossRef]
14. Shuai, Z.; Liu, D.; Shen, J.; Tu, C.; Cheng, Y.; Luo, A. Series and parallel resonance problem of wideband frequency harmonic and its elimination strategy. *IEEE Trans. Power Electron.* **2014**, 1941–1952. [CrossRef]
15. Wang, L.; Lam, C.; Wong, M. Minimizing inverter capacity design and comparative performance evaluation of SVC-coupling hybrid active power filters. *IEEE Trans. Power Electron.* **2019**, *34*, 1227–1242. [CrossRef]
16. Wai, R.; Zhang, Q.; Wang, Y. A novel voltage stabilization and power sharing control method based on virtual complex impedance for an off-grid microgrid. *IEEE Trans. Power Electron.* **2019**, *34*, 1863–1880. [CrossRef]
17. Hao, Q.; Man, J.; Gao, F.; Guan, M. Voltage limit control of modular multilevel converter based unified power flow controller under unbalanced grid conditions. *IEEE Trans. Power Del.* **2018**, *33*, 1319–1327. [CrossRef]
18. Zhao, X.; Zhang, C.; Guo, X.; Xiu, H.; Jia, D.; Shi, C.; Wei, T. Novel power flow analysis method based on impedance matching for UPQC with grid voltage fluctuations and unbalanced loads. *IET Power Electron.* **2020**, *13*, 4417–4427. [CrossRef]
19. Zhang, C.; Zhao, X.; Wang, X.; Xiu, H.; Zhang, Z.; Guo, X. A grid synchronization PLL method based on mixed second- and third-order generalized integrator for DC-offset elimination and frequency adaptability. *IEEE J. Emerg. Sel. Top. Power* **2018**, 1517–1526. [CrossRef]
20. Zhao, X.; Zhang, C.; Chai, X.; Zhang, J.; Liu, F.; Zhang, Z. Balance control of grid currents for UPQC under unbalanced loads based on matching-ratio compensation algorithm. *J. Mod. Power Syst. Clean Energy* **2018**, *6*, 1319–1331. [CrossRef]
21. Pelza, G.M.; Silvab, S.A.O.; Sampaiob, L.P. Comparative analysis involving PI and state-feedback multi-resonant controllers applied to the grid voltage disturbances rejection of a unified power quality conditioner. *Int. J. Electr. Power* **2018**, *6*, 1517–1526. [CrossRef]
22. Ghosh, A.; Banerjee, S.; Sarkar, M.K.; Dutta, P. Design and implementation of type-II and type-III controller for DC–DC switched-mode boost converter by using K-factor approach and optimisation techniques. *IET Power Electron.* **2016**, *9*, 938–950. [CrossRef]
23. Modesto, R.A.; Silva, S.A.O.; Oliveira, A.A.; Bacon, V.D. A versatile unified power quality conditioner applied to three-phase four-wire distribution systems using a dual control strategy. *IEEE Trans. Power Electron.* **2016**, *31*, 5503–5514. [CrossRef]
24. Chen, Y.; Zhang, B. Minimization of the electromagnetic torque ripple caused by the coils inter-turn short circuit fault in dual-redundancy permanent magnet synchronous motors. *Energies* **2017**, *10*, 1798. [CrossRef]